Hindawi
Shock and Vibration
Volume 2022, Article ID 8679189, 8 pages
https://doi.org/10.1155/2022/8679189

Research Article

Quasi-Static Test Study on Seismic Behavior of Large-Section Fabricated Utility Tunnel

Li Zhu,[1] Shiqing Shangguan,[2] Haitao Yu,[3] Yawei Guo,[4] Zheng Chen,[5] and Dong An[5]

[1]*CCCC-SHEC Engineering Design and Research Institute, Xi'an 710065, China*
[2]*CCCC Highway Consultants Co., LTD Shanghai Branch, Shanghai 200082, China*
[3]*Key Laboratory of Geotechnical and Underground Engineering of Ministry of Education, Tongji University, Shanghai 200092, China*
[4]*CCCC Highway Bridges Nationals Engineering Research Centre CO. Ltd., Beijing 100120, China*
[5]*School of Civil Engineering, North China University of Technology, Beijing 100144, China*

Correspondence should be addressed to Zheng Chen; imcz54cz@163.com

Received 29 December 2021; Accepted 26 February 2022; Published 18 March 2022

Academic Editor: Xuepeng Zhang

Based on the urban utility tunnel project in Xiong'an New Area, to clarify the seismic behavior of the utility tunnel structure, the overall structure model of the four-cabin large-section utility tunnel and the quasi-static test of the joint specimens have been completed. The results show the following. (1) The hysteresis curve of the overall structure is relatively full, showing good ductility and energy consumption. The middle joint has better bending performance. The ductility of the side joint is worse than that of the middle one. (2) The skeleton curve of the joint specimen is divided into three stages: obvious cracking, yielding, and ultimate load. After the overall structure reaches the ultimate load, the load curve basically tends to be horizontal. (3) The stiffness degradation of the overall structure and the joint specimens continues to be uniform during the entire loading process. (4) The structural design of the fabricated utility tunnel can ensure the seismic behavior under normal condition.

1. Introduction

Urban utility tunnel has the advantages of ensuring the safety of municipal pipelines, improving the utilization rate of underground space, beautifying the urban environment, and avoiding repeated excavation of pavement. Xiong'an New Area has complex underground traffic, including comprehensive pipe network, drainage pipe network, rail transit, gas, heating (cooling), and water supply and drainage pipe network. The prefabricated utility tunnel scheme is adopted. Scholars carried out a lot of research on the seismic behavior of utility tunnels.

Tsinidis et al. [1] provided a summary of relevant experimental studies that took place in the centrifuge or on shaking tables, discussed analytical models, simplified methods, and numerical schemes for the seismic analysis of tunnels. In China, shaking table tests were conducted on a 1 : 8 scaled utility tunnel model under nonuniform input earthquake excitation [2–4]. Seismic response characteristics and earthquake damage mechanism of utility tunnel system were explored. The two-span structure size is 6000 mm × 2500 mm [5]. The behavior of utility lined tunnels under single and multiple earthquakes is studied by the finite element method [6]. Static concentric load test was performed on the full-scale model to study the failure mechanism, bearing capacity, and crack condition of the structure of the utility tunnel without axillary angle [7]. There were a lot of studies on tunnel nodes. The crack development situation of seven kinds of tunnel nodes was obtained under monotonic static load [8]. Han et al. studied two kinds of double box utility tunnels: with and without joint connections via shaking table model tests [9]. With the construction of a utility tunnel in the 2010 Shanghai Expo as the background, monotonic static tests were conducted using full-scale models of joint and structure to investigate the mechanical properties of the precast tunnel [10].

The finite element software ABAQUS was utilized to establish a three-dimensional finite element model of a single-compartment rectangular utility tunnel. The dynamic response analysis of the utility tunnel structure suffering different seismic waves was carried out [11]. Three types of precast tunnel connections are investigated by the numerical model [12, 13].

The research object of this paper is the fabricated utility tunnel with the largest cross section and the largest hoisting tonnage in China. The fabricated utility tunnel has a large transverse span, buried depth, and complex stress during operation. In this study, the dead load in normal service state is applied to the utility tunnel, and the low-cycle loading is carried out on the side joint, middle joint, and overall structure of the utility tunnel structure respectively. The failure mode, load-displacement hysteretic curve, load-displacement skeleton curve, stiffness degradation, and energy consumption of the joint and overall structure are obtained, which provides a reference for the design and application of the fabricated utility tunnel.

2. Test Situation

2.1. Design and Fabrication. The dimensions of the fabricated utility tunnel studied in this paper are shown in Figure 1. The section width is 15800 mm, the height is 4750 mm, and the length of the longitudinal section is 6000 mm. The utility tunnel structure consists of four cabins [14], namely, gas cabin, utility cabin, and two power cabins, in which the width of the gas cabin is 2850 mm, the width of utility cabin is 4050 mm, the width of power cabin 1 is 4750 mm, the width of power cabin 2 is 2150 mm, and the height of each cabin is 3750 mm. The thickness of the top plate is 400 mm, and the bottom plate is 600 mm. C40 waterproof concrete which is widely used in China is adopted [15, 16]. The steel bar adopted for the middle span of the top and bottom plate of the utility tunnel is HRB400 whose tensile strength is 400 MPa, which diameter is 28 mm and spaced 150 mm.

The seismic test includes two parts: joint specimen and integral specimen. Middle and side joints are taken for joint specimens. The middle joint specimen is the middle wall of the utility cabin and power cabin 1, and the side joint specimen is the left wall of the gas cabin. The dimensions are all in 1/2 scale, and the width of the joint specimen is 1000 mm. Figures 2(a) and 2(b) show the size of the two joint specimens, respectively. The overall test specimen is 1/4 scale, the length is 3950 mm, the width is 1500 mm, and the height is 1175 mm. Figure 2(c) is the photo of the overall specimen.

2.2. Test Loading Scheme. The loading device is composed of vertical and horizontal MTS actuators, pull rods, distribution beams, anchor bolts, and anchor beams. The vertical load is applied to the top plate of the wall panel to simulate the superstructure and overburden weight under the actual working condition, and the horizontal low-cycle load is applied to the top of the side wall of the specimen to simulate the seismic action [17]. The specimen is anchored on the ground with anchor beam and bolt. To ensure uniform stress, the MTS actuator is connected with the distribution beam, which is connected to the specimen as a whole through the pull rod. The loading scheme is shown in Figure 3.

Under the maximum water level loading condition in the normal condition, the surface load transmitted by the superstructure is 0.13 MPa, and the load applied by the vertical actuator is 767 kN after calculation. The surface load on the top surface corresponding to the middle joint and side joint specimens is 0.94 MPa and 0.51 MPa, respectively. After calculation, the loading applied by the vertical actuator of the middle joint and side joint specimens is 376.8 kN and 127.8 kN, respectively.

Preload before the test to ensure that the test specimens are stable, the data acquisition and load equipment are normal, the load is continuous and uniform, and the load and unloading speed is consistent. Load control shall be adopted before the specimen yield. The load of each level shall be repeated once, which shall be loaded three times to close to the cracking load, and then, the differential load shall be reduced until the crack is observed. After that, 10% of the ultimate load shall be loaded each time, and the extreme difference shall be reduced before approaching the yield load. The deformation control is adopted after the specimen yields. The deformation value is the maximum displacement at yield, and the displacement value is used as the level difference for control, repeated twice. Load to 85% of the ultimate loading as the falling section of the test curve.

2.3. Layout of Measuring Points. The horizontal displacement and horizontal load of the load point are measured and recorded during the test. High precision displacement sensors are arranged at the key parts of the test specimens to record the horizontal displacement, and the sensors at the end of the MTS actuator measure the horizontal load. During each stage of loading and holding, the cracking of the test specimens is recorded through the crack card.

3. Test Result

3.1. Crack Development and Failure Mode

3.1.1. Internal Joint. When the middle joint was loaded to 90 kN, cracks were generated. When it was continuously loaded to 220 kN, new longitudinal cracks were generated, and some longitudinal cracks developed to the full length along the longitudinal direction. Near the yield load, cracks appear on the side, the crack width develops, and cracks appear in the core area. After that, displacement control was adopted. When the forward load is up to 36 mm and the reverse load is up to -56 mm, the longitudinal crack and the crack width in the core area continued to develop, and the crack in the core area gradually extended into the wall and bottom plate. When the final loading stopped at 84 mm, the concrete on the surface of the core area continues to peel off, resulting in typical core area failure. The failure mode of the middle joint is shown in Figure 4(a).

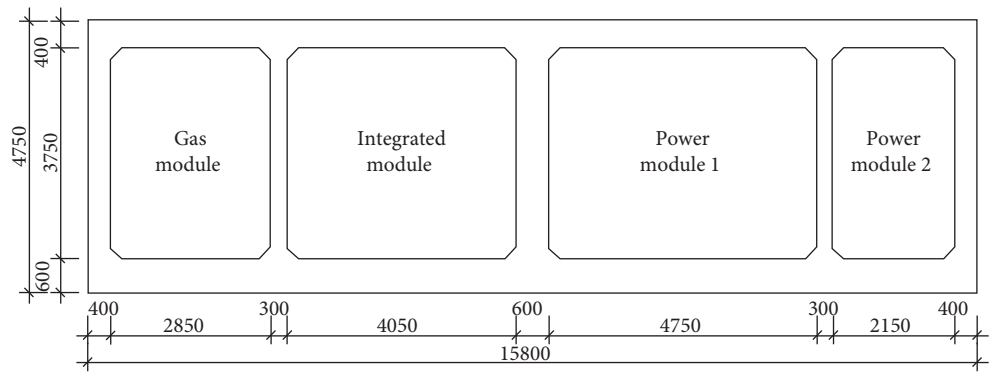

Figure 1: Schematic diagram of the utility tunnel (unit: mm).

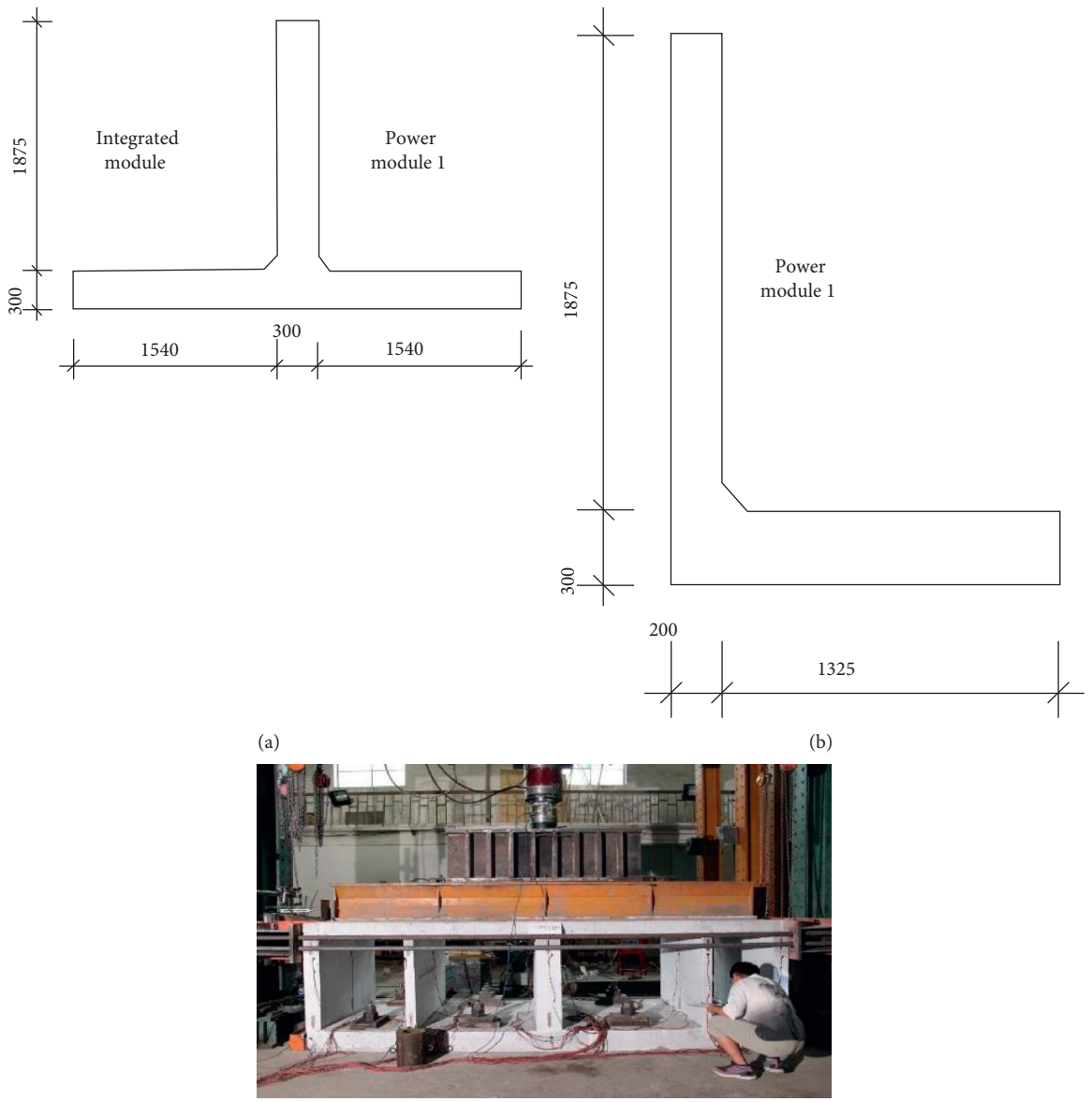

Figure 2: Joint specimen size and integral photo: (a) middle joint specimen; (b) side joint specimen; (c) overall specimen (unit: mm).

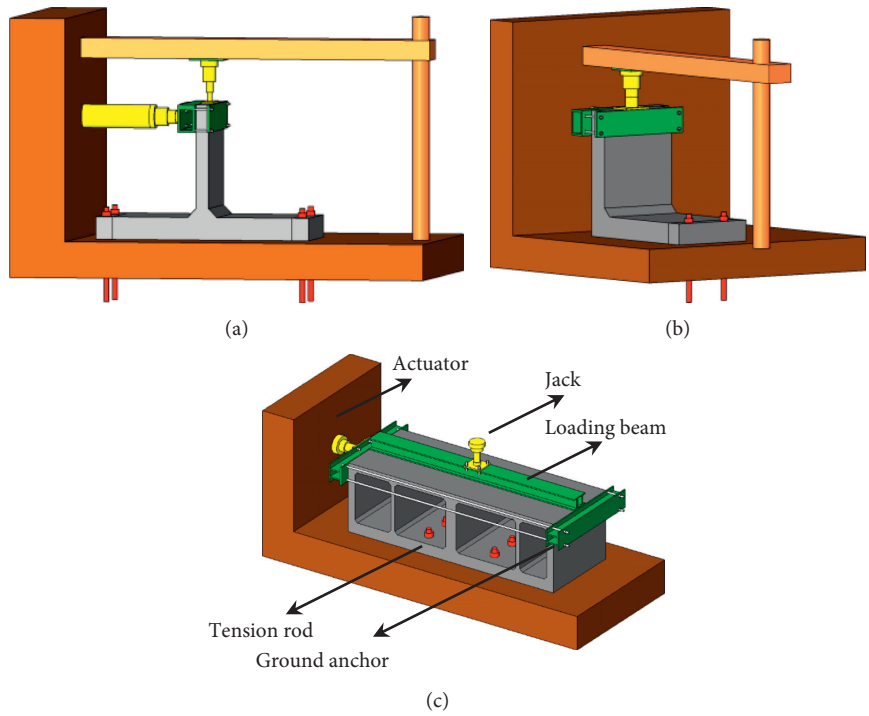

Figure 3: Schematic diagram of loading: (a) middle joint specimen; (b) side joint specimen; (c) overall specimen.

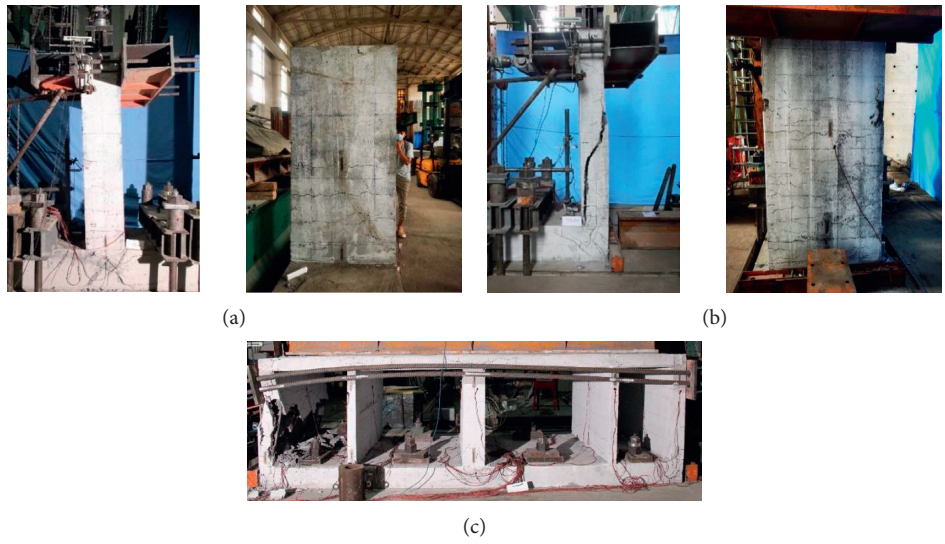

Figure 4: Joint failure mode: (a) middle joint specimen; (b) side joint specimen; (c) overall specimen.

3.1.2. Side Joints. When the side joint specimen was loaded to 20 kN, it would produce cracks, and when the positive load was 90 kN, it would produce new longitudinal cracks and gradually develop to the full length along the longitudinal direction. When it was close to the yield load, there would be cracks on the side. Then, the displacement control was adopted. In the process of positive load to 30–40 mm, the longitudinal cracks would continue to produce or develop and become wider obviously. The cracks in the core area continue to develop. When the displacement was loaded to 39 mm and −49 mm, respectively, the cracks in the plastic hinge area were obvious and produced vertical cracks. In the process of loading to 40–70 mm, the cracks continued to expand, and the concrete damage was obvious. Finally, when the negative load from 70 mm to − 55 mm, the wall of the specimen was sheared. Because of the asymmetry of structure and reinforcement, the difference between positive and negative loading is obvious. In practice, there are lateral Earth pressure and water pressure, which

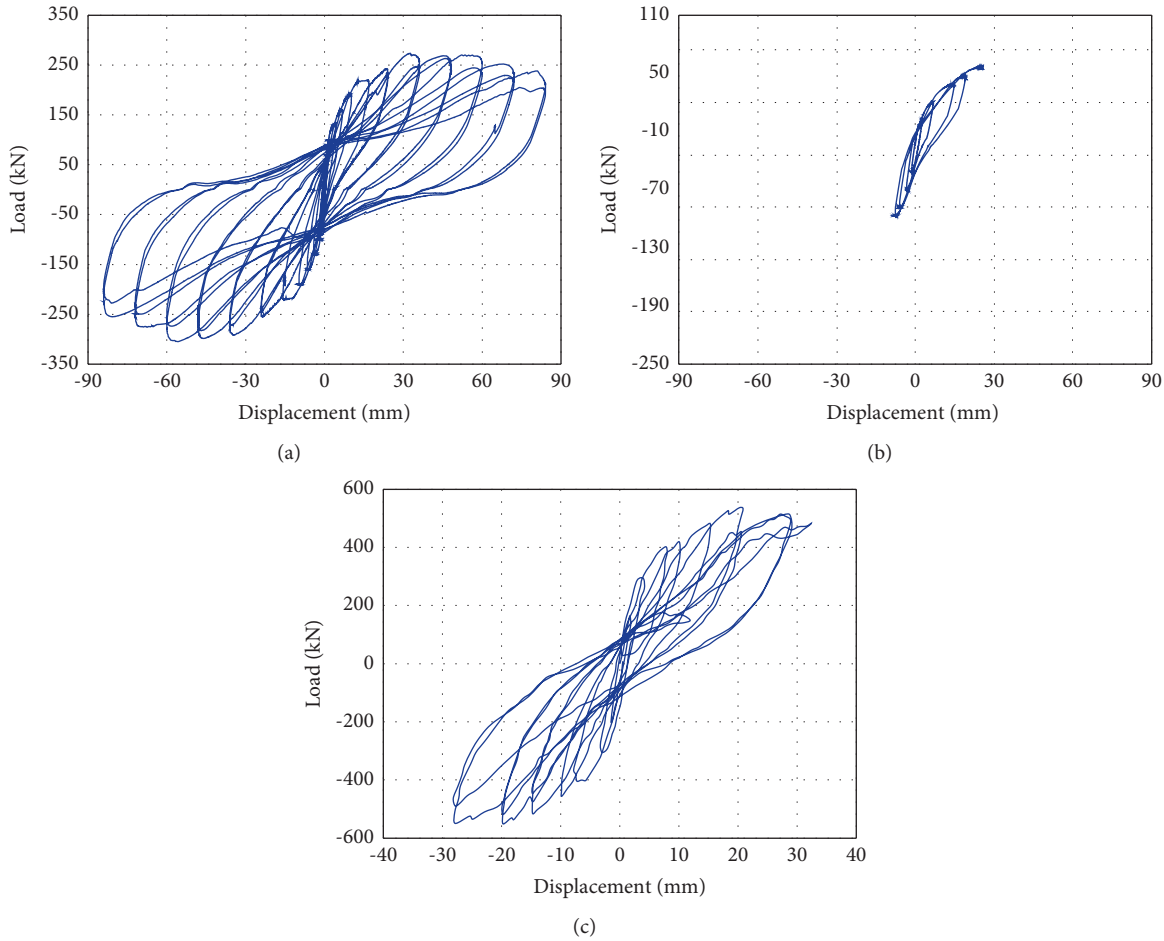

Figure 5: Horizontal load-displacement hysteresis curve of loading point: (a) middle joint; (b) side joint; (c) overall structure.

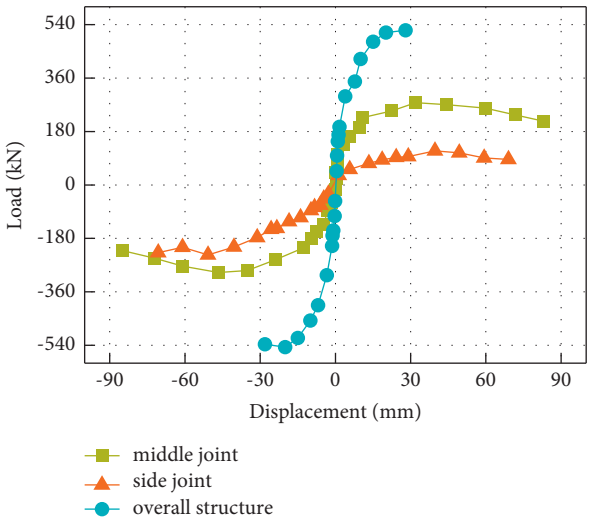

Figure 6: Horizontal load-displacement skeleton curve.

can alleviate this asymmetry. The side joint specimen continues to load after the limit stage of the specimen, and a maximum crack appears, resulting in the shear failure of the wall, which belongs to brittle failure. See Figure 4(b), for the failure mode of side joints.

3.1.3. Overall Structure. Cracks appear when the overall structure was loaded to 170 kN, and new longitudinal cracks appear when it was continuously loaded to 400 kN and gradually develop to the full length along the longitudinal direction. Cracks appear in the side core area when it was close to the yield load. During the loading process from 7 mm to 20 mm by displacement control, the longitudinal cracks continue to develop and widen, and the cracks in the core area continue to develop. When the displacement was loaded to 20 mm, the cracks in the plastic hinge area were obvious, vertical cracks were generated, and the concrete in the core area was spalling. The wall on the left side of the specimen is sheared when the load was continued to about 28 mm. The overall failure of the utility tunnel was the loss of bearing capacity of the components, the shape of the core area of the joint was intact, but many side wall concrete was peeled off, indicating that the structure of the concrete comprehensive utility tunnel meets the stress requirements. The failure mode of the overall structure is shown in Figure 4(c).

3.2. Hysteretic Curve. The horizontal load-displacement hysteretic curves of specimens are shown in Figure 5. It can be seen from the figure that the hysteretic curves of each

Table 1: Characteristic displacement and load of specimen.

Specimen	Load direction	P_y/kN	Δ_y/mm	P_m/kN	Δ_m/mm	Δ_u/mm	μ
Middle point	Positive	213.80	12.10	273.24	32.54	72.12	5.96
	Negative	−217.90	−12.17	−304.68	−55.74	−71.89	5.91
Side point	Positive	97.27	27.36	114.95	38.94	50.00	1.83
	Negative	−164.81	−25.10	−239.14	−49.33	−59.70	2.39
Overall structure	Positive	350.00	7.73	542.00	20.056	28.00	3.62
	Negative	−400.00	−7.00	−547.50	−20.056	−28.00	4.00

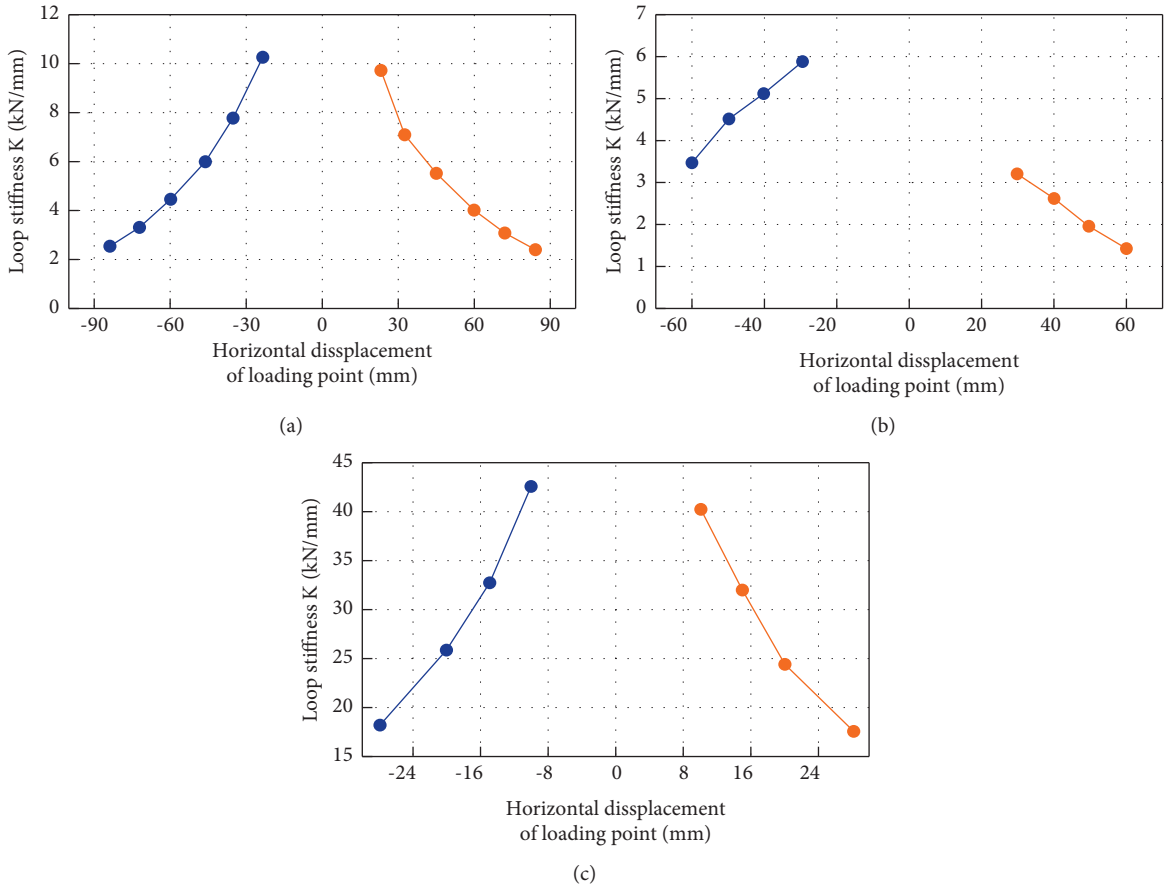

Figure 7: Stiffness degradation curve: (a) middle joint; (b) side joint; (c) overall structure.

specimen are relatively full, showing good ductility and energy dissipation capacity. The middle joint has more obvious stability than the side joint in the later stage of loading. The middle joint has better flexural performance, ductility, and energy dissipation capacity. The hysteretic curve of side joints is not full due to the asymmetry of structure and reinforcement, and the ductility is worse than that of middle joints. The hysteretic curve of the whole structure is complete and full.

3.3. Skeleton Curve. The skeleton curves under horizontal load are shown in Figure 6. The skeleton curves of the middle joint and side joint specimens are divided into three stages: obvious cracking, yield, and limit. After the curve enters the descending section, it can still maintain a certain load. After cracking the whole specimen, the skeleton curve has an inflection point. After reaching the ultimate load, the curve basically tends to be horizontal, and the structure reaches the limit state of bearing capacity.

The characteristic loads and displacements of the test pieces are given in Table 1. Displacement ductility coefficient μ is the ratio of the ultimate displacement Δ_u and yield displacement Δ_y, where the ultimate displacement Δ_u is the displacement corresponding to the load decreasing to 85% P_m (P_m is the ultimate load) [17]. It can be seen from the table that the positive and negative ultimate loads of the middle joint and the overall specimen are basically equal, and the positive and negative properties of the side specimen are naturally asymmetric due to the asymmetry of its structure and reinforcement. The displacement ductility coefficients of joint and integral structure specimens are basically more than 2.0, and the ductility is good.

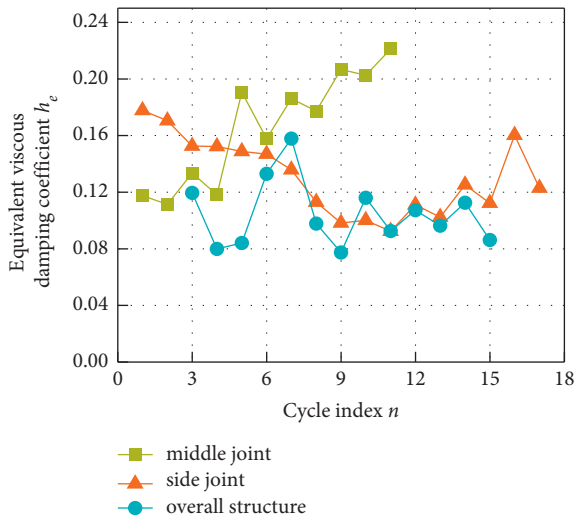

Figure 8: Equivalent viscous damping coefficient.

3.4. Stiffness Degradation. The stiffness degradations of each specimen are shown in Figure 7. There is little difference between the positive and negative stiffness degradation of the middle joint and the overall specimen, but there is a large difference between the positive and negative stiffness of the side joint specimen. The stiffness degradation of each specimen is continuous, uniform, and stable during the whole loading process.

3.5. Energy Dissipation Capacity. The energy dissipation capacity of the specimen is usually measured by the area surrounding of the load-displacement hysteretic curve. The equivalent viscous damping coefficient is generally used to characterize the energy dissipation characteristics of the specimen [15]. The equivalent viscous damping coefficient cycle index curves of each specimen are shown in Figure 8.

4. Conclusions

Through the quasi-static test study of the seismic behavior of the utility tunnel structure, the analysis shows that

(1) Typical core failure occurred in the middle joint specimens. The biggest crack in the side joint specimen leads to the shear failure of the wall, which belongs to brittle failure. The concrete of the overall structure of the utility tunnel has less tensile plastic damage and compressive plastic damage, and the plastic deformation capacity of the structure is very strong, indicating that the structure of the concrete comprehensive utility tunnel meets the stress requirements;

(2) The hysteretic curves of the whole structure and joint specimens are relatively full, showing good ductility and energy dissipation capacity. The hysteretic curve of side joints is not full due to the asymmetry of structure and reinforcement, and the ductility is worse than that of middle joints.

(3) The skeleton curve of the joint specimen can still maintain a certain load after entering the descending section. After the whole specimen reaches the ultimate load, the curve can maintain the horizontal.

(4) Although the positive and negative stiffness of the side joint specimens are greatly different due to symmetry, the stiffness degradation is stable throughout the loading process. The stiffness degradation is small, and the seismic behavior of the overall structure is good.

Data Availability

The data used to support the findings of this study are included within the article.

Conflicts of Interest

The authors declare that they have no conflicts of interest.

References

[1] G. Tsinidis, F. de Silva, I. Anastasopoulos et al., "Seismic behaviour of tunnels: from experiments to analysis," *Tunnelling and Underground Space Technology*, vol. 99, Article ID 103334, 2020.

[2] X. Shi, J. Chen, and J. Li, "Shaking table test on underground utility tunnel," *Earthquake Engineering and Engineering Vibration*, vol. 28, no. 06, pp. 116–123, 2008.

[3] J. Chen, X. Shi, and J. Li, "Shaking table test of utility tunnel under non-uniform earthquake wave excitation," *Soil Dynamics and Earthquake Engineering*, vol. 30, no. 11, pp. 1400–1416, 2010.

[4] J. Chen, L. Jiang, J. Li, and X. Shi, "Numerical simulation of shaking table test on utility tunnel under non-uniform earthquake excitation," *Tunnelling and Underground Space Technology*, vol. 30, pp. 205–216, 2012.

[5] A. P. Tang, Z. Q. Li, R. C. Feng, and X. Y. Zhou, "Model experiment and analysis on seismic response of utility tunnel systems using a shaking table," *Journal of Harbin Institute of Technology*, vol. 41, no. 06, pp. 1–5, 2009.

[6] L. Wu, Y. Su, J. Chen, J. X. Han, Q. W. Mao, and D. S. Wang, "Three-dimensional finite element analysis on the seismic response of the single chamber rectangular utility tunnel and its experimental verificatio," *Journal of Civil Engineering and Management*, vol. 38, no. 03, pp. 51–58, 2021.

[7] W. J. Yi, L. Yan, and Z. Peng, "Static load test and finite element analysis on full-scale model of utility tunnel structure without axillary angle," *Journal of Hunan University*, vol. 46, no. 07, pp. 1–10, 2019.

[8] Z. X. Tian, *Experimental Research on Force Performance of Precast concrete Underground Comprehensive Municipal Tunnel*, Harbin Institute of Technology, China, 2016.

[9] L. Han, H. Liu, W. Zhang et al., *Seismic Behaviors of Utility Tunnel-Soil System: With and without Joint Connections*, Underground Space, vol. 6, pp. 1–14, 2021.

[10] X. Hu and W. C. Xue, "Experimental study of mechanical properties of PPMT," *China Civil Engineering Journal*, vol. 43, no. 05, pp. 29–37, 2010.

[11] F. D. Konstandakopoulou, N. D. Beskou, and G. D. Hatzigeorgiou, "Three-dimensional nonlinear response of utility tunnels under single and multiple earthquakes," *Soil Dynamics and Earthquake Engineering*, vol. 143, no. 4, Article ID 106607, 2021.

[12] H. Qian, J. Li, Z. Zong, C. Wu, and Y. Pan, "Behavior of precast segmental utility tunnel under ground surface Explosion: a numerical study," *Tunnelling and Underground Space Technology*, vol. 115, Article ID 104071, 2021.
[13] H. Qian, Z. Zong, C. Wu, J. Li, and L. Gan, "Numerical study on the behavior of utility tunnel subjected to ground surface explosion," *Thin-Walled Structures*, vol. 161, Article ID 107422, 2021.
[14] GB 50838-2015, *Technical Code for Urban Comprehensive Utility Tunnel Engineering*, (in Chinese), 2015.
[15] GB 50010-2010, *Design Code for concrete Structures*, (in Chinese), 2010.
[16] GB 50011, *Code for Seismic Design of Buildings*, (in Chinese), 2010.
[17] JGJ/T101, *Building Seismic Test Code*, (in Chinese), 2015.